Magnetocaloric studies of the peak effect in Nb

N. D. Daniilidis,* I. K. Dimitrov, V. F. Mitrović, C. Elbaum, and X. S. Ling†
Department of Physics, Brown University, Providence, Rhode Island 02912, USA
(Received 30 October 2006; revised manuscript received 24 January 2007; published 21 May 2007)

We report a magnetocaloric study of the peak effect and Bragg glass transition in a Nb single crystal. The thermomagnetic effects due to vortex flow into and out of the sample are measured. The magnetocaloric signature of the peak-effect anomaly is identified. It is found that the peak effect disappears in magnetocaloric measurements at fields significantly higher than those reported in previous ac-susceptometry measurements. Investigation of the superconducting-to-normal transition reveals that the disappearance of the bulk peak effect is related to inhomogeneity broadening of the superconducting transition. The emerging picture also explains the concurrent disappearance of the peak effect and surface superconductivity, which was reported previously in the sample under investigation. Based on our findings, we discuss the possibilities of multicriticality associated with the disappearance of the peak effect.

DOI: 10.1103/PhysRevB.75.174519 PACS number(s): 74.25.Qt, 74.25.Op, 61.12.Ex

I. INTRODUCTION

One very fascinating result in condensed-matter physics in recent decades is the understanding that, in spite of early predictions,[1] the long-range topological order associated with broken continuous symmetries can survive in systems with random pinning.[2,3] In bulk type-II superconductors with weak pointlike disorder, the existence of a novel Bragg glass phase has been predicted.[3] This reaffirmed experimental facts known since the 1970s that vortex lattices in weak-pinning, bulk, type-II superconductors can produce pronounced Bragg peaks in neutron diffraction.[4] Recent experiments[5,6] have shown that a genuine order-disorder transition occurs in vortex matter. This transition appears to be the underlying mechanism of the well-known anomaly of the peak effect[7] in the critical current near H_{c2}. However, there are still many outstanding issues concerning the Bragg glass phase boundary and the nature of the disordered vortex state above the peak effect.

Previous studies in a niobium single crystal have revealed an intriguing picture of the peak effect in weakly pinned conventional superconductors. Neutron scattering has shown that a vortex lattice order-disorder transition occurs in the peak-effect region. This transition shows hysteresis and is believed to be first order, separating a low-temperature ordered phase from a high-temperature disordered one.[5] The hysteresis was not observed across the lower field part of the superconducting-to-normal phase boundary. Magnetic ac susceptometry showed that at lower fields, the peak effect disappears as well, indicating further connection between the peak effect and the order-disorder transition.[8] In addition, the line of surface superconductivity H_{c3} terminates in the vicinity of the region where the peak effect disappears. This picture is summarized in Fig. 1.

It was thus proposed that the peak effect is the manifestation of a first-order transition which terminates at a multicritical point (MCP) where the peak-effect line meets a continuous, Abrikosov transition, H_{c2}. The MCP would be bicritical if a third line of continuous transitions ends there. The transition lines considered as a possible third candidate were a continuous vortex glass transition T_{c2} and the line of surface superconductivity. Alternatively, the MCP would be tricritical if the disordered phase is a pinned liquid with no high-field transition into the normal state.[8] Subsequently, the disappearance of the peak effect at low fields has also been reported in other systems.[9,10]

Thermodynamic considerations[8] suggest that the MCP is likely a bicritical point. Since bicriticality implies the existence of competing types of order in the vortex system, the question of which of the two lines T_{c2} or H_{c3} is relevant to the bicritical point has major importance. Its answer will provide insight into the disordered vortex state above the peak effect and the disordering transition itself. Evidently, the possible relevance of surface superconductivity to the destruction of bulk Bragg glass ordering, and hence the existence of the multicritical point, cannot be dismissed *a priori*. In fact, it is well known that surface premelting plays an important role in solid-liquid transitions.[11]

This issue could be resolved by repeating the ac magnetic susceptibility measurements after having suppressed surface superconductivity with appropriate surface treatment. Our efforts to nondestructively achieve this, e.g., by electroplating the sample surface with a ferromagnetic layer, proved unfruitful, possibly due to high oxygen content of the surface.

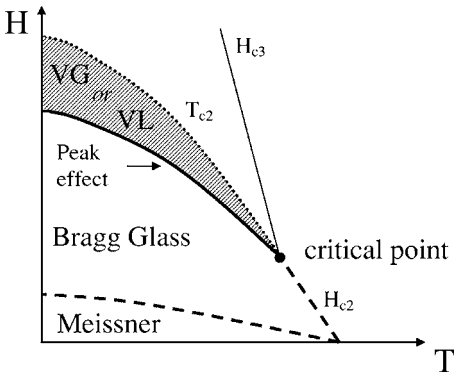

FIG. 1. A sketch of the phase diagram of the Nb single crystal from Park *et al.* (Ref. 8). The nature of the phase in the shaded region remained undetermined, VG being a vortex glass, and VL a vortex liquid phase. Note the definitions of distinct T_{c2}, H_{c2}, and peak-effect lines.

Here, we report a study of the peak effect using a magnetocaloric technique. Clear features associated with the peak effect have been identified in the magnetocaloric data. We find that the superconducting-to-normal transition shows inhomogeneity broadening at all fields. The peak effect in the bulk critical current is found to disappear when it enters into the inhomogeneity broadened transition region. It is concluded that the concurrent disappearance of surface superconductivity and the peak effect is likely due to interference of surface superconductivity with the ac-susceptibility measurements. Nevertheless, the location of the MCP, as determined from magnetocaloric measurements, is in close vicinity to the location previously reported.[8] Moreover, the transition across T_{c2} seems to be the same as that at H_{c2}, and surface superconductivity plays only a coincidental role in the critical point. This result suggests that the disordered vortex state, which is represented by the shaded part in Fig. 1, is a distinct thermodynamic phase. Bicriticality implies that this phase has an order parameter competing with that of the Bragg glass phase.

The paper is organized as follows. In Sec. II, we review the basic principle of magnetocaloric measurements and give the experimental details of the sample and the technique used. In Sec. III, we present our main results and proceed to the interpretation of the data. Finally, we summarize our findings and conclusions and propose experimental work necessary to address the issues raised. A technical discussion of irreversible and nonequilibrium effects is given in the Appendix.

II. EXPERIMENT

A. The magnetocaloric measurement technique

1. General features and basic principle

In studies of vortex phases in bulk superconductors, various experimental techniques provide complementary pieces of information. Combining these in a complete picture is a nontrivial task. Magnetization measurements offer information comparable to magnetocaloric measurements but are not practical for large bulk samples. Magnetic ac-susceptibility measurements are sensitive to screening currents, and thus to the location of peak-effect features, but are not suitable for the identification and study of the H_{c2} transition itself.[8] Calorimetric[12,13] and ultrasonic attenuation[14,15] measurements determine the upper critical field where bulk condensation of Cooper pairs occurs, but it remains unclear under what circumstances they also provide a peak-effect signature. The combination of information obtained with different techniques has to rely on thermometry. Furthermore, the dynamical measurements can suffer from thermal gradients in the studied samples. Magnetocaloric measurements overcome these difficulties because they are sensitive to both the presence of bulk superconductivity and to dynamical, flux-flow related effects. Moreover, they can be performed in quasiadiabatic conditions, where virtually no thermal gradients are present in the sample. Finally, they can be easily performed using a common calorimeter.

The magnetocaloric effect is a special case of thermomagnetic effects in the mixed state of superconductors which have long been known and investigated.[16] These arise from the coexistence of the superconducting condensate which is not involved in entropy-exchange processes for the superconductor and the quasiparticles, localized in the vortex cores, which are entropy carriers. Due to the presence of localized quasiparticles in the vortex cores, vortex motion results in entropy transport, which causes measurable thermal effects. Specifically, during field increase, new vortices are created at the edge of the sample, and quasiparticles inside the vortices absorb entropy from the atomic lattice and cause quasiadiabatic cooling of the sample. Conversely, during field decrease, the exiting vortices release their entropy to the atomic lattice, causing quasiadiabatic heating.

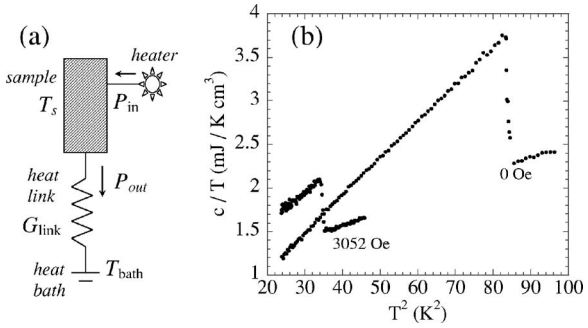

FIG. 2. (a) Idealized heat-flow diagram of the calorimeter used. (b) Specific heat of Nb crystal at 0 and 3052 Oe. The superconducting transition width is approximately 83 mK. A small contribution from the addenda of the calorimeter is included in c.

A superconductor subject to a changing magnetic field and allowed to exchange heat with the environment undergoes a temperature change. This process is described by the first law of thermodynamics:

$$dQ_{abs}/dt = nT_s(\partial s/\partial H)_T dH/dt + nC_s dT_s/dt, \qquad (1)$$

where dQ_{abs}/dt is the net rate of heat absorption, positive for absorption of heat by the sample, n is the molar number of the superconductor, T_s its temperature, $T_s(\partial s/\partial H)_T$ the molar magnetocaloric coefficient, and C_s the specific heat of the superconductor.

A schematic of our setup is represented in Fig. 2(a). In this setup, absorption or release of heat from the sample results in minute, but measurable, variation of its temperature. In a typical measurement, the sample temperature is first fixed at a selected value T_{s0}. Subsequently, the field is ramped at a steady rate, resulting in quasiadiabatic absorption or release of heat from the sample. The resulting sample temperature change is recorded. In our setup, $dQ_{abs}/dt = -G_{link}\Delta T$, where $T_s = T_{s0} + \Delta T$ is the sample temperature. The magnetocaloric term in Eq. (1) induces the temperature change. This is smeared out by the last term, incorporating the effect of specific heat. Nevertheless, in practice, this last term is constrained to be negligible when magnetocaloric effects are measured. In our measurements, we use very low field ramp rates (dH/dt), which result in very low-temperature change rates (dT_s/dt) causing the last term to be negligible.[17]

Under this condition, the temperature change of the sample (ΔT) around its static value T_{s0} allows us to determine the molar magnetocaloric coefficient $T_s(\partial s/\partial H)_T$ by use of

$$-G_{\text{link}}\Delta T = nT_s(\partial s/\partial H)_T dH/dt, \quad (2)$$

where the sample temperature, differential thermal conductance of the heat link G_{link}, molar number for the sample n, and field ramp rate dH/dt are all independently measured. The latter is positive for increasing fields, and negative for decreasing fields.

2. Irreversible and nonequilibrium effects

In deriving the above equations, we assumed that heat is only exchanged between the superconductor and the environment and that the superconductor reaches its quasistatic state as the measurement is performed. In an actual experiment, nonequilibrium and irreversible effects need to be considered. The heat generated by the dissipative processes, friction, between the vortex lattice and atomic lattice leads to a modification of the left-hand side of Eqs. (1) and (2). Nonequilibrium effects related to pinning and surface barriers lead to a modification of the right-hand side. While the effects of the Bean-Livingston surface barrier,[18] flux-flow heating,[19] and the Bean critical state[20] can be complex and subtle, a detailed analysis has been performed and is discussed in the Appendix. In concluding this section, we note that since Eq. (2) describes an idealized process, in what follows, we refrain from using $(\partial s/\partial H)_T$ to symbolize the quantity related to the magnetocaloric temperature change ΔT. Instead, we choose (ds/dH) to symbolize the measured entropy derivative.

B. Sample and setup

We used a Nb single-crystal sample with mass of 24.78 g, which was previously studied using small-angle neutron scattering (SANS) and ac susceptometry.[5,8] It has an imperfect cylindrical shape (radius of 0.5 cm, length of 2.47 cm) with the cylinder axis oriented parallel to the [111] crystallographic direction. It has a T_c of 9.16 K and upper critical field $H_{c2}(0) \approx 5600$ Oe, as previously reported.[5,8] We performed a zero-field specific-heat measurement, as shown in Fig. 2(b). This was done with the heat-pulse (relaxation) technique. From this measurement, we obtain the Ginzburg-Landau parameter $\kappa(0)=3.8$, which is higher than the previous estimate.[8] In addition, we find a superconducting transition width of 83 mK. The residual resistivity ratio from 300 to 10 K is measured to be 12, suggesting a significant amount of defects in this Nb crystal. This is consistent with the large κ and upper critical-field values.

Our experimental setup is a homemade calorimeter and its idealized heat-flow diagram is shown in Fig. 2(a). It consists of an oxygen-free, high-purity copper can which serves the role of a heat bath surrounding the sample. A piece of high-purity copper wire is used as a heat link between the sample and heat bath and the mechanical support for the sample is provided by nylon rods. During measurements, the heat bath is maintained at a temperature of 4.20 K and a carbon glass thermometer (Lakeshore) monitors its temperature. A second thermometer (Cernox, Lakeshore) is directly attached with silver epoxy to the lower end of the sample for reading the sample temperature. To minimize electronic noise in reading the thermometer resistance, a 10 kHz sinusoidal excitation together with phase-sensitive detection is used. A Manganin wire, which is noninductively wound on the sample and secured with 1266 Stycast epoxy, serves as a heater. A 50-turn high-purity copper coil is directly wound on the sample for ac magnetic susceptibility measurements. During measurements, the vacuum in the calorimeter is maintained to lower than 1 mTorr Hg by use of activated charcoal in thermal contact with the helium bath.

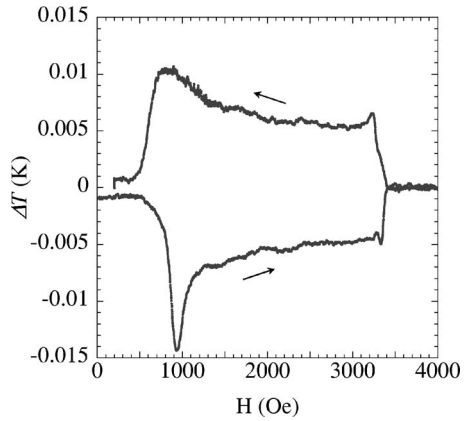

FIG. 3. Magnetocaloric temperature variation around $T_{s0}=5.37$ K vs applied field for increasing and decreasing field. The field ramp direction is indicated by arrows. $dH/dt=0.92$ Oe/s was used.

The calorimetric measurements of Fig. 2(b) were performed with the standard heat-pulse technique. This technique offers moderate resolution and is not suited for studying the thermodynamics of the peak effect. For example, no features were detectable at the peak effect in an applied field of 3052 Oe. Nevertheless, these measurements allow us to characterize our sample. In Fig. 2(b), we also show the data acquired in zero applied field, from which we derived the sample properties quoted above.

During magnetocaloric measurements, a constant heat input P_{in} is supplied to the sample through the Manganin heater, fixing the temperature at a selected static value T_{s0}. After the sample temperature has stabilized to T_{s0}, the magnetic field is ramped up and then down at a constant rate. During a field ramp, the sample temperature as a function of field $T_s(H)$ is recorded. The magnetocaloric signal $\Delta T(H)$ has to be measured with respect to a *field dependent*, static sample temperature *reading* $T_{s0}=T_{s0}(H)$, the thermometer reading at field H in the absence of field ramping. In other words, one has to determine $\Delta T(H)=T_s(H)-T_{s0}(H)$. An example of raw data, ΔT vs H, is shown in Fig. 3.

The field dependence of the $T_{s0}(H)$ thermometer reading is a result of the following two effects: first, the magnetoresistance of the thermometer used, and second, a changing temperature gradient across the sample, as its field dependent thermal conductivity changes. This gradient can become con-

siderable in the Meissner state for the highest measured temperatures (≈8 mK/cm at 8.33 K). Nevertheless, it is negligible (less than 0.5 mK/cm) in the peak effect region, which is the main focus of this paper. We stress here that the thermal gradient is a result of the external heat input P_{in}, and not of the magnetocaloric effect.

A possible variation of the heat input with applied field, resulting from magnetoresistance of the heater, was investigated. It was verified that the heat input from the manganin heater does not vary by more than one part in 10^4 for the entire field range covered in any of our measurements.

The differential thermal conductance of the heat link between the sample and heat bath, G_{link}, to be used in Eq. (2) above is also measured at all temperatures of interest for the entire range of applied fields. The link conductance is found to vary smoothly by no more than one part in 100 for the entire field range studied. This variation is insignificant compared to the random noise in the raw ΔT data and shall not be considered further.

Finally, the field ramp rate is measured through a resistor connected in series with the magnet coil, which allows us to monitor the current through the magnet. For all of the measurements presented here, the ramp rate is 0.92 Oe/s, which is the lowest possible with our system. At higher ramp rates, for example, 1.87 Oe/s, giant flux jumps were found to occur in the sample.

III. RESULTS AND DISCUSSION

A. Magnetocaloric results

1. Main features in field scans

In Figs. 4(a) and 4(b), we summarize the molar entropy derivative (ds/dH) measurements on (a) increasing and (b) decreasing fields at different temperatures. (ds/dH) is calculated from the $T_s(H)$ data following the procedure outlined above.

As indicated for the lowest-temperature curve, 4.83 K [the upper most curve in Fig. 4(a)], several important features deserve attention. On increasing fields, a peak occurs at low field. This is marked by H_1. It corresponds to the lowest field for vortex entry through a surface barrier. Its locus on the H-T plane closely follows the thermodynamic field $H_c(T)$ but occurs slightly lower. This behavior is expected for a sample with finite demagnetizing factor and mesoscopic surface irregularities.[21] It should be emphasized that the field H_1 is larger than the lower critical field $H_{c1}(T)$. No peak corresponding to H_1 is present on decreasing fields. Rather, a smoother increase of (ds/dH) occurs as the field is lowered, before entry of part of the sample into the Meissner state where the magnetocaloric signal vanishes, as seen in Figs. 3 and 4(b).

In intermediate fields, we identify a feature which was not observed in previous magnetic susceptibility studies.[8] This appears as a knee in (ds/dH), which shows larger negative slope as a function of field for fields lower than H_{knee}, as illustrated in Fig. 4(c). The feature is the same for both field-ramp directions. With our setup, we can identify the H_{knee} feature up to 7.41 K. As the temperature is increased, the region between H_1 and H_{c2} narrows and it becomes increasingly difficult to discern H_{knee}. Thus, it is unclear how this feature terminates, i.e., whether it ends on the H_{c2} line at around $H=1000$ Oe or if it continues to lower fields.

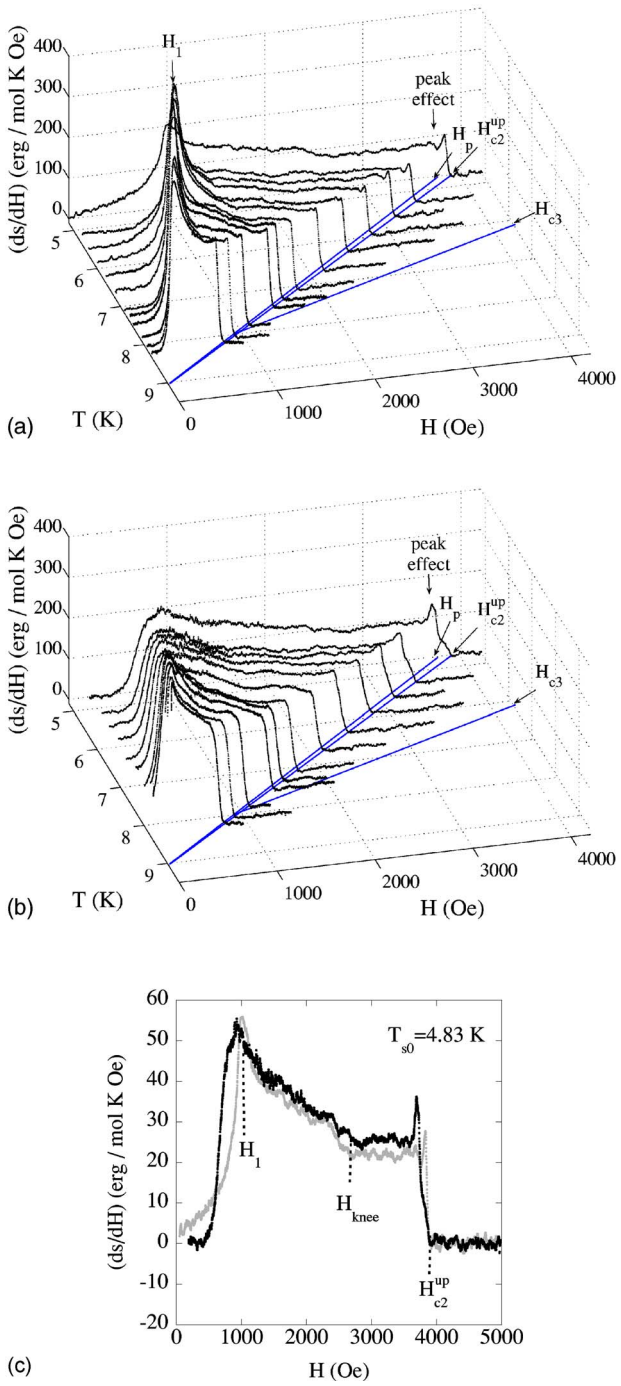

FIG. 4. (Color online) Results of magnetocaloric measurements on (a) increasing and (b) decreasing fields. Also shown (in blue) are the loci traced on the H-T plane by H_p, H_{c2}^{up}, and H_{c3}. The H_{c3} line is drawn according to Park *et al.* (Ref. 8). (c) Full field scan at $T_{s0}=4.83$ K. Gray: Increasing field. Black: Decreasing field. The fields H_1 and H_{knee} and the upper limit of the upper critical field are marked.

At high field, across H_{c2}, the equilibrium mean-field theory of Abrikosov predicts a step function for $(\partial m/\partial T)_H$.[22] Thus, in the simplest picture, one would expect a simple step of the molar entropy derivative $(\partial s/\partial H)_T$ at H_{c2}. Instead, we observe that across the peak-effect regime, complex features of valley and peak appear in (ds/dH) below the field marked H_{c2}^{up}. The valley in (ds/dH) corresponds to the peak effect, as indicated in Fig. 4. Similar features appear on decreasing the field. At fields above the peak effect, the disappearance of the magnetocaloric effect marks the upper critical field H_{c2}. As we will soon discuss, the upper critical field shows inhomogeneity broadening. In Fig. 4, we mark with H_{c2}^{up} the upper end of the upper critical field. This is the value of field at which the magnetocaloric signal in the mixed state exceeds the normal-state noise level. Our technique is not sensitive to H_{c3} effects and the data are featureless above H_{c2}^{up}.

2. Identification of the peak effect

To verify the identification of the peak effect in our measurements, we performed simultaneous magnetocaloric and ac-susceptibility measurements, as shown in Fig. 5(a). In the quasiadiabatic magnetocaloric setup, the ac amplitude used has to be small. For large amplitudes, inductive heating occurs in the mixed state and the sample temperature increases rapidly by several degrees *as the peak effect is crossed*. We used an amplitude of 0.5 Oe at 107 Hz as a compromise between feasibility of the magnetocaloric measurement and resolution in the χ' results. The results are shown in Fig. 5(a).

In this combined measurement, we find that both the onset and the peak of the peak effect have corresponding features. Moreover, we find no clear change in χ' when the upper critical field, determined from the magnetocaloric measurement, is crossed. A slight change occurs in the slope of the $\chi'(H)$ curve across H_{c2}, but significant amount of screening, caused by surface superconductivity, remains when the bulk of the sample is in the normal state. This is a typical example of the inadequacy of ac susceptometry in determining the upper critical field. Even with the use of larger ac fields, the change in slope of $\chi'(H)$ turns into a shoulder which does not reveal the exact location or characteristics of the bulk superconducting transition.[8]

3. Features of the peak effect

In light of the first-order transition underlying the peak effect,[5] it is tempting to interpret the peak appearing in (ds/dH) at the peak effect as a manifestation of the entropy discontinuity of the transition. Nevertheless, a simpler interpretation is offered in the context of critical state[20] induced, nonequilibrium magnetization during the field ramps.

We start with increasing field data. At temperatures below 6.79 K where the peak effect is observed, the magnetocaloric signal starts dropping at the onset H_{on} of the peak effect. A minimum occurs in the vicinity of the peak of the peak effect H_p and it is followed by a peak, see Fig. 5(b). This indicates slowing down, and then acceleration of vortex entry into the sample, as the critical state profile becomes steep, and then levels, in the peak-effect region. Finally, the magnetocaloric signal gradually drops to zero in the region of the upper critical field.

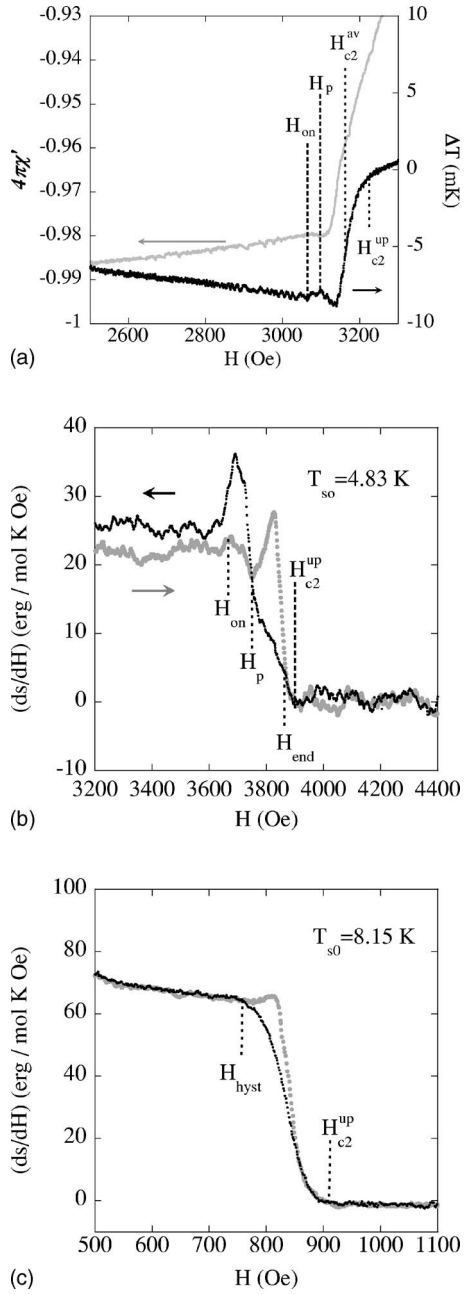

FIG. 5. (a) Magnetocaloric temperature variations and ac magnetic susceptibility as a function of increasing field at $T=5.76$ K. The peak effect in χ' is not pronounced due to the small ac amplitude used ($h_{ac}=0.5$ Oe, $f=107$ Hz). (b) Detail of magnetocaloric measurement in the upper critical-field region at $T=4.83$ K. Gray: Increasing field. Black: Decreasing field. (c) Same as (b) but at $T=8.15$ K.

On decreasing field, a magnetically reversible region is revealed to exist for fields between H_{end} (the "end" of the peak effect) and H_{c2}^{up}. This is shown in Fig. 5(b). Such behavior can be understood keeping in mind that the upper critical field in our sample is characterized by inhomogeneity broadening. We believe that the sliver of magnetic reversibility corresponds to the appearance of superconducting islands in

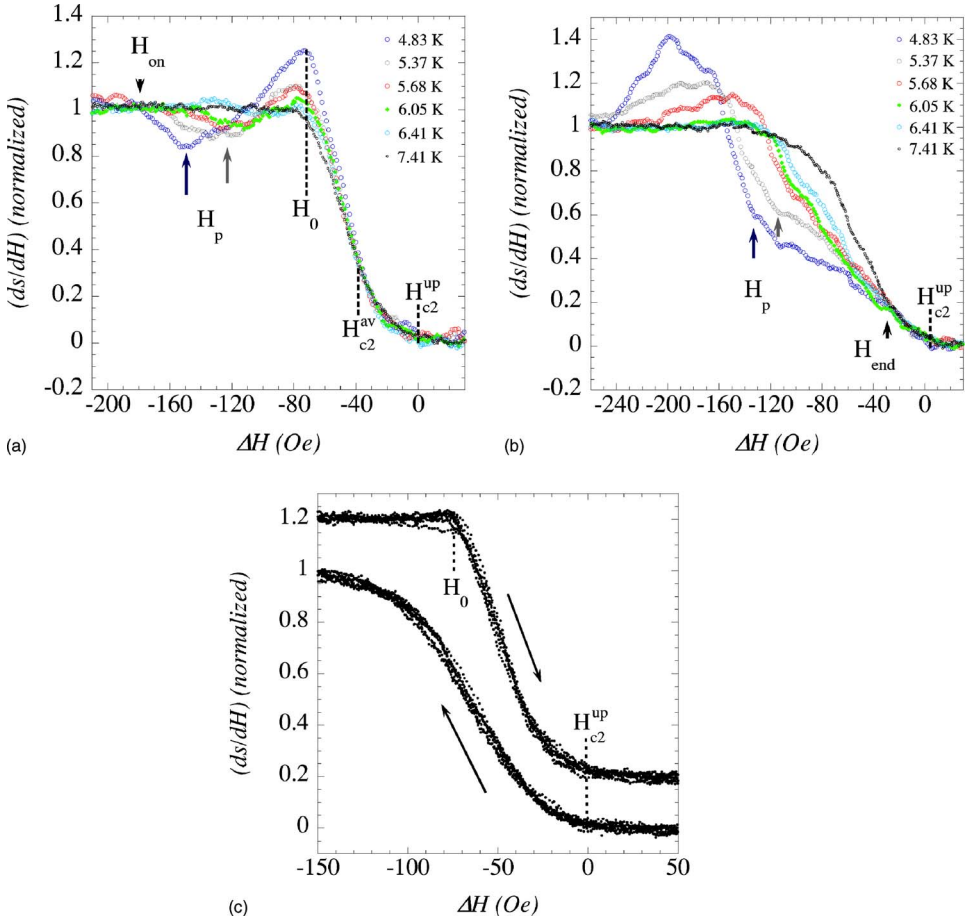

FIG. 6. (Color online) Normalized entropy derivative (ds/dH) versus $\Delta H = H - H_{c2}^{up}$ for the magnetocaloric data in the upper critical-field region. (ds/dH) is rescaled to unity in the ΔH region between −300 and −250 Oe. (a) Increasing field data with and without the peak effect. The 7.41 K data do not show peak effect. The upper critical field shows inhomogeneity broadening between fields H_0 and H_{c2}^{up}. (b) Same as a for decreasing field. (c) Collapsed magnetocaloric curves without peak effect for increasing (top, vertically offset by +0.2) and decreasing (bottom) fields. Temperatures included: 7.18, 7.41, 7.55, 7.94, 8.15, and 8.33 K.

our sample. These give rise to magnetocaloric effects, but they are isolated within the bulk and cannot support a screening supercurrent around the circumference of the sample, hence the reversible behavior. The end of the peak effect marks the onset of irreversibility and corresponds to a shoulder in the decreasing field curve. This occurs when continuous superconducting paths form around the sample and a macroscopic critical current is supported. As the field is lowered below H_{end}, flux exit is delayed due to the increase in critical current. When $H < H_p$, the critical state profile relaxes and accelerated flux exit results in the observed peak in (ds/dH) below H_p.

4. (ds/dH) peak in absence of peak effect

In both field-ramp directions, the features due to the peak effect become less pronounced with increasing temperature and finally disappear even before the previously identified[8] critical point is reached. On increasing fields, for $T > 7.18$ K, a new peak appears in (ds/dH) just below the critical field, as shown in Fig. 5(c). A similar feature has already been reported in calorimetric measurements in pure Nb and Nb_3Sn.[12,23] It has been attributed to critical fluctuations in the superconducting order parameter which set in as the critical field is approached.[24] If this is the cause of the observed peak, we expect it to exist in the curves displaying the peak-effect features, but its presence will be obscured by the dramatic results of nonequilibrium magnetization discussed above. Interestingly, a similar peak is *not* observed on the decreasing field data, Fig. 5(c). It is evident in Fig. 5(c) that apart from hysteretic behavior, over an approximately 100 Oe wide region between H_{hyst} and H_{c2}^{up}, the behavior of the sample is reversible to within noise levels. We attribute this to critical state flux screening in opposite field-ramp directions. The hysteresis occurs consistently at all temperatures where the peak effect is not observed.

5. The superconducting-to-normal transition region

A very striking feature of our data is the invariance of the shape of the transition into (or out of) the bulk normal state with changing temperature, or critical field. For increasing fields, the transition into the normal state occurs between the fields H_0 and H_{c2}^{up}, where (ds/dH) drops to zero monotonically. To illustrate this, in Fig. 6, we show the *normalized* entropy derivatives as a function of field for temperatures

ranging from 4.83 to 8.33 K, with an expanded view of the upper critical-field region. The normalization has been performed such that the average of $(ds/dH)_n$ over a 50 Oe wide region below the onset of the peak effect equals unity. The curves have also been horizontally offset on a $\Delta H=H-H_{c2}^{\mathrm{up}}$ axis. The horizontal alignment can alternatively be performed by aligning the ordinate of either H_0 or the part of the curve where the signal equals a given value, for example, 0.1 in the normalized Y axis. All different criteria result in alignments differing by only a few oersteds. The case is similar for decreasing fields.

In Fig. 6(a), we present increasing field data that display the peak effect on the normalized and/or offset axes. For comparison, one curve which does not display the peak effect has been included. This corresponds to $T=7.41$ K. In Fig. 6(b), we present the corresponding decreasing field data. In Fig. 6(c) we show only curves without a peak effect for both increasing and decreasing fields. These figures illustrate the uniform characteristics of the transition between the mixed state and the normal state. This is most evident in Fig. 6(c): All different curves collapse onto one uniform curve for each field-ramp direction. In Figs. 6(a) and 6(b), the occurrence of the peak effect results in variations of the magnetocaloric signal around this uniform transition. These variations are, as already discussed, consistent with critical state induced flux screening on the field ramps. The uniformity of the transition for all field values implies that critical fluctuation broadening of the transition plays a minor role in our sample. Rather, inhomogeneity broadening seems to be the cause for the observed behavior.

For increasing fields the gradual disappearance of the magnetocaloric signal in the region between H_0 and H_{c2}^{up} corresponds to the gradual loss of bulk superconductivity in our sample. In all of our measurements, the width $H_{c2}^{\mathrm{up}}-H_0$ is essentially constant around a mean of 74.1 ± 1.9 Oe [Figs. 6(a) and 6(c)], which translates to a width of 78.8 ± 2.0 mK on the temperature axis. This value is in good agreement with that obtained in the calorimetric measurement (83 mK, Sec. II), given the finite temperature step of 10–15 mK used in the latter. Based on the identification of the lower and upper limits of the upper critical field, we identify the location of the mean-field transition H_{c2}^{av} to be in the midpoint of the H_0 to H_{c2}^{up} range, see Fig. 6(a). Local variations in electronic properties in the sample cause the broadening around this value.

The width of the superconducting transition is significantly larger than the expected lowest Landau-level fluctuation broadening of the transition given by $\Delta T_{fl} \approx 10\delta = 10\left(\frac{k_b}{8\pi\xi_0^3\Delta c(T)}\right)^{2/3}\left(\frac{T}{T_c(0)}\right)^{1/3}\left(\frac{B}{T_c(0)dH_{c2}/dT}\right)^{2/3}$ $T\approx 20$ mK at 4000 Oe.[23,24] Consequently, it is not surprising that no broadening of the transition is observed with increasing field.

B. Discussion

1. Disappearance of the peak effect in (ds/dH)

We already mentioned that in the magnetocaloric measurements, the peak effect disappears for temperatures above 7.18 K, or critical fields H_{c2}^{av} below 1718 Oe. However, in previous χ' ac-susceptometry measurements on the same sample, the peak effect was found to occur for fields as low as 900 Oe.[8] We believe that this discrepancy is a result of the two different techniques used. Magnetocaloric measurements probe bulk flux changes and critical currents in the sample, while ac susceptometry is more sensitive to effects occurring near the surface.

We will see that the peak effect disappears in the magnetocaloric measurement when it crosses into the region where only parts of the sample are normal. This occurs in the vicinity of 1700 Oe. It is not clear whether the bulk peak effect continues to exist for lower fields. It seems likely that it becomes undetectable due the absence of bulk macroscopic critical current in the partially superconducting sample. However, the peak effect continues to manifest in ac susceptibility.[8] This is not surprising, since surface superconductivity assists in the formation of current-supporting, superconducting paths near the sample surface, even when such paths do not exist in the bulk [cf. Fig. 5(a)]. This argument also provides an explanation for the approximately simultaneous disappearance of the peak effect and surface superconductivity in previous work.[8]

In order to follow the disappearance of the peak effect in magnetocalorics, one can trace the evolution of the positions of the onset and peak features in our increasing field data. We focus on increasing fields, because in these the range of the upper critical-field transition between H_0 and H_{c2}^{up} is clearly discernible. The locations of H_0 and H_p are each identified by the intersection of two linear fits on different sections of the (ds/dH) curve. Each fit is performed in a limited ΔH range on either side of the turning point where the feature occurs. For example, H_p is defined by the intersection of two linear fits to the data, one roughly in the range of H_{on} to H_p and one in the range of H_p to H_0.

Following this procedure, we construct an H-T diagram of the observed features. In Fig. 7(a), we show the positions of H_1, H_{knee}, H_p, and H_{c2}^{av} in H vs T axes. We also indicate the position of the MCP identified by Park *et al.*[8] In Fig. 7(b), we focus on the region of the peak effect. For this reason, we choose ΔH vs H_{c2}^{av} axes. We mark the positions of the onset, the peak, and the end of the peak effect, as well as the lower end (H_0) and the midpoint (H_{c2}^{av}) of the H_{c2} transition. It is evident in this more detailed figure that the peak effect disappears when it crosses over into the H_0 to H_{c2}^{up} range, where bulk superconductivity is partially lost due to sample inhomogeneity.

These results also support the previously proposed multicriticality picture (Sec. I and Park *et al.*[8]). The observation with ac susceptometry of a continuation of the bulk peak-effect line on the surface of the sample is an indication that the peak effect continues to exist in isolated superconducting islands inside the sample, despite the existence of normal regions. Moreover, as shown in Fig. 7, the linear extrapolation of the onset and the peak of the peak effect, as well as H_{c2}^{av}, merge at a field of approximately 850 Oe, suggesting that this may indeed be the vicinity of the critical point where the first-order phase transition underlying the peak effect ends.

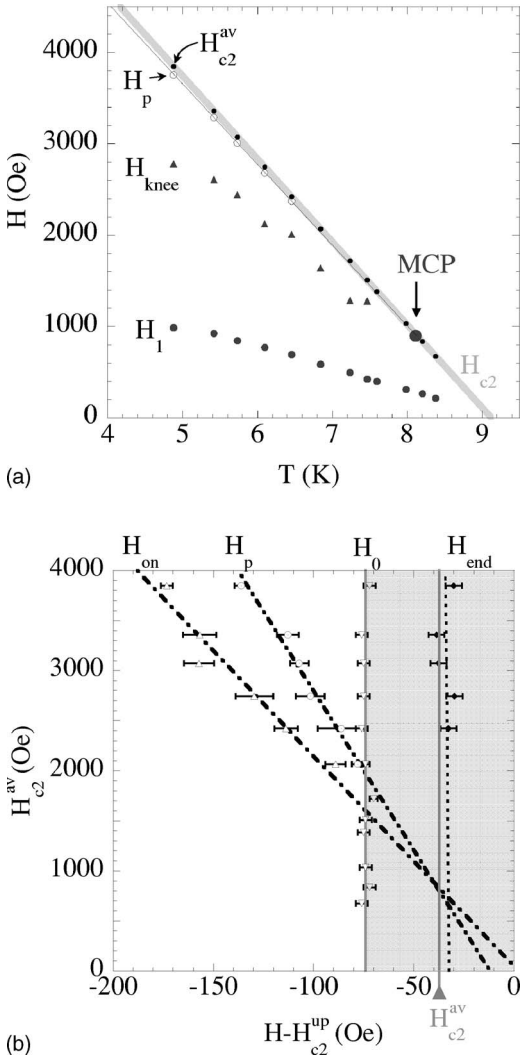

FIG. 7. Phase diagram obtained from magnetocaloric measurements. (a) The identified features in *H-T* axes. The thin solid line and wide shaded line are linear fits through H_p and H_{c2}^{av}. The width of the H_{c2} line represents the extent of inhomogeneity broadening. The location of the MCP after Park *et al.* is indicated. (b) Detail of the upper critical-field region: distance of various features from the conventionally defined H_{c2}^{up} line vs H_{c2}^{av}. The shaded area corresponds to the upper critical-field region.

2. The H_{c2} and T_{c2} transition lines

The nature of the MCP which was previously identified by Park *et al.*[8] remained unresolved. As discussed, our findings suggest that surface superconductivity plays only a coincidental role in the disappearance of the peak effect. Thus, the nature of the MCP is determined from the nature of the H_{c2} and T_{c2} lines mentioned in Sec. I.

We have a means of comparing the H_{c2} and T_{c2} transitions. The approximate location of the MCP in ac susceptometry is at $T=8.1$ K, $H=900$ Oe. Yet, as mentioned, the peak effect disappears in magnetocaloric measurements in the neighborhood of 7.0 K, 1700 Oe on the (T,H) plane. This allows us to compare the magnetocaloric transitions into the bulk normal state on the two sides of the MCP. As shown in Fig. 6(c), all the curves with $H_{c2}^{av}<1718$ Oe (or equivalently

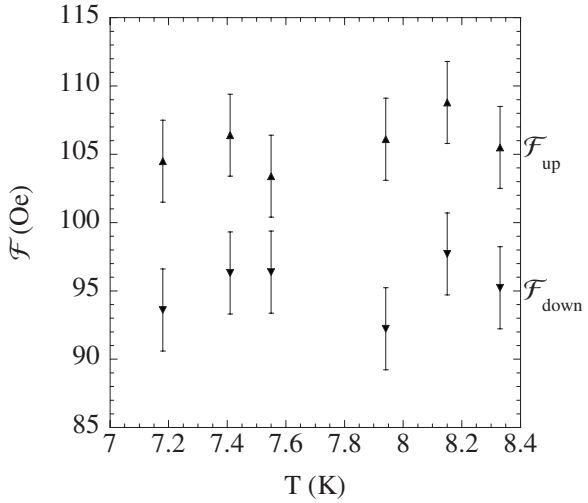

FIG. 8. Integrals of $(ds/dH)_n$ for ΔH from −150 Oe to 30 Oe for increasing ($\mathcal{F}_{up}$, ▲) and decreasing ($\mathcal{F}_{down}$, ▼) fields. The peak-effect feature was not observed at these temperatures. The error bars reflect the uncertainty in alignment of the magnetocaloric curves. Temperatures above 8.15 K correspond to the H_{c2} line of transitions indicated by Park *et al.* (Ref. 8).

$T>7.18$ K) for both increasing and decreasing fields collapse strikingly on two different curves. These data include transitions on both sides of the MCP. This suggests that the phase transitions out of the Bragg glass (H_{c2}) and disordered (T_{c2}) phases are of the same nature. In other words, well defined vortices exist in the disordered vortex state above the peak effect. Here, "well defined" is taken to mean that their magnetocaloric signature is indistinguishable from the one obtained in the transition between the normal and the Bragg glass phases. However, it has to be borne in mind that changes in critical behavior can be subtle and hard to identify in our sample which shows significant inhomogeneity broadening.

We can overcome this difficulty and look for changes in critical behavior by integrating the normalized experimental curves, $(ds/dH)_n$. This way, a change or a trend in critical behavior obscured by inhomogeneity broadening will be more easily discernible as a trend in the computed integrals. The computed integrals of the normalized increasing ($\mathcal{F}_{up}$) and decreasing ($\mathcal{F}_{down}$) field curves around the region of the upper critical field are plotted in Fig. 8. The integration has been performed between limits −150 Oe and 30 Oe in the offset axis, ΔH. More explicitly,

$$\mathcal{F}=\int_{-150}^{30}\left(\frac{ds}{dH}\right)_n d(\Delta H).$$

The error bars arise from the uncertainty in choosing H_{c2}^{up}. All temperatures refer to the T_{c2} transition, except for the two higher ones which correspond to H_{c2}. We see no systematic trend in neither $\mathcal{F}_{up}$ nor $\mathcal{F}_{down}$ in any of the available temperatures. In conclusion, as far as the inhomogeneity of our sample allows us to discern, there is no detectable change

between the low-field H_{c2} transition and the high-field T_{c2} transition to the normal state.

3. End of the peak effect

We turn to the end of the peak effect. Its position in the phase diagram is shown in Fig. 7(b). H_{end} occurs in a range between 32 and 39 Oe below H_{c2}^{up}. H_{end} has been identified as the field at which a continuous superconducting network which can support a macroscopic screening supercurrent forms inside the sample. We note that it occurs slightly above the midpoint of the H_0 to H_{c2}^{up} range, as shown in Fig. 7(b). This indicates that the critical current appears when roughly half of the sample is in the mixed state while the rest is still in the normal state. This observation is very interesting but requires further investigation. The role of surface superconductivity in establishing macroscopic supercurrents in the superconducting network can be examined experimentally.

4. The "knee" feature

Finally, we return to the identified knee feature, shown in Fig. 4(c). From the occurrence of the knee in both ramp directions, we conclude that it corresponds to an equilibrium feature of the thermodynamic behavior inside the Bragg glass phase. To appreciate this argument, note that all three sources of irreversible and nonequilibrium effects discussed in the Appendix will induce asymmetry on the (ds/dH) curves for opposite field-ramp directions. For example, the two curves of Fig. 4(c) show asymmetry consistent with that in Figs. 9(a) and 9(b), discussed in the Appendix. This is due to surface barrier-related heating on increasing field. On the other hand, symmetric trends in the measured (ds/dH) curves have to be related to equilibrium behavior, and we thus conclude that H_{knee} corresponds to an equilibrium feature. Neutron scattering did not reveal any structural changes in the vortex lattice[5,8] in the region of H_{knee}, which suggests that the nature of this feature is rather subtle. It would be interesting to investigate the corresponding part of the phase diagram for changes in dynamical response, as well as for a possible relation of this feature to the thermomagnetic instability in Nb.

C. Summary and discussion

In this work, we identified the magnetocaloric signature of the peak effect on the Nb crystal previously studied with SANS and ac susceptometry.[5,8] The observed behavior is consistent with a previous report[25] on Nb_3Sn. Our data allow us to correlate the evolution of the peak effect with other aspects of the superconducting phase diagram of this sample.

The upper critical field had previously been proposed to consist of two distinct lines of transitions, the low-field H_{c2} and high-field T_{c2}.[8] In ac-susceptometry measurements, there is no clear signature of T_{c2}. Our magnetocaloric measurements here indicate that the low-field transition from the Bragg glass phase into the normal state (H_{c2}) is of the same nature as the high-field transition between the structurally disordered[5] vortex state and the normal state (T_{c2}). The widths of both transitions do not increase with increasing field, which is indicative of inhomogeneity broadening. In magnetocaloric measurements, the peak effect disappears in the H-T phase diagram at low fields, but at a field value considerably higher than that found in ac susceptometry.

The ac-susceptometry measurement is sensitive to the screening current near the surface, which is assisted by a superconducting surface layer. Thus, the simultaneous disappearance of H_{c3} and H_p in ac susceptometry is not related to the proposed MCP. In addition, the observation of a peak effect near the sample surface with ac susceptometry indicates that at low fields, the peak effect occurs in the bulk of the sample in the isolated regions that are superconducting. The H_{on}, H_p, and H_{c2}^{av} lines in our data extrapolate to a location in close vicinity to the MCP proposed by Park *et al.*[8]

Our results have strong implications for understanding the nature of the multicritical point where the peak effect disappears.[8–10] A tricritical point can be ruled out since the change in slope between the H_p and low-field H_{c2} lines would lead to violation of the thermodynamic 180° rule.[8,26] The fact that the magnetocaloric transition appears to be continuous and of the same character across both T_{c2} and H_{c2} suggests that the critical point is bicritical. Bicriticality implies competing order parameters in the two bulk vortex phases. In our case, these are the ordered Bragg glass[2,3] and a disordered vortex glass. The vortex glass phase is not necessarily superconducting in the sense of the original proposal,[27] but it has to be a genuine phase possessing an order parameter absent in the normal state, and *in competition* with that of the Bragg glass.[28] Alternatively, in the absence of a MCP, the region of the phase diagram between H_p and T_{c2} may be attributed to a dirty vortex state of the Griffiths type.[29,30]

The peak effect consistently occurs slightly below T_{c2}. It is pronounced in a region where no lowest Landau level (LLL) fluctuation effects[24] were observed or expected. For example, at 3850 Oe the peak effect occurs more than 100 Oe below H_{c2}^{av} and 60 Oe below H_0. These translate to distances of more than 100 and 60 mK on the temperature axis, far outside the LLL fluctuation region for this field,[24,31] given by $\Delta T_{fl} \approx 20$ mK. We thus attribute the peak effect in our sample to a disorder-driven order-disorder transition of the vortex lattice.[32] In recent work, the peak effect in Nb_3Sn (Ref. 12) and $NbSe_2$ (Ref. 33) has been found to occur in the regime of strong LLL fluctuations, close to the upper critical field. We attribute the suppression of the peak-effect transition temperature in our sample to increased level of disorder. The Bragg glass disordering transition, just like melting of a crystalline solid, can be thermally driven or disorder driven, with increased disorder leading to lowering of the melting temperature.[34]

ACKNOWLEDGMENTS

We thank J. J. Rush and J. W. Lynn from NIST for providing the Nb crystal and acknowledge numerous helpful discussions with D. A. Huse, J. M. Kosterlitz and M. C. Marchetti. This work was supported by NSF under Grant No. NSF-DMR 0406626.

APPENDIX: IRREVERSIBLE AND NON-EQUILIBRIUM EFFECTS

Here we evaluate the results of nonequilibrium and irreversible processes in the magnetocaloric measurements.

We start with the surface barrier. Its presence results in delay of flux entry into the sample on increasing fields, up to a field approximately equal to the thermodynamic critical field, H_C.[21] In addition, the surface barrier has the more subtle consequence of introducing an asymmetry between the measured ΔT on increasing and decreasing fields. On increasing fields, vortices have to enter the sample through an energy barrier in a vortex free region.[35,36] In this process, entry of individual vortices to the bulk of the sample results in energy dissipation of: $\Phi_0[(H_C^2+H^2)^{1/2}-H]/4\pi$ per vortex unit length.[35] For the entire sample, energy is dissipated approximately at a rate

$$\Phi_0[(H_C^2+H^2)^{1/2}-H](V/4\pi)(dH/dt),$$

where V is the sample volume and H_C the thermodynamic critical field.

In our measurements, for example, at $H \approx 3000$ Oe, this amounts to approximately 2 μW, and will reduce the (negative) ΔT observed on increasing fields by roughly 1 mK. On decreasing fields, the surface barrier has essentially no effect, and no irreversible heating is expected.[35] An asymmetry of this kind is shown schematically in Fig. 9(a) and it is present in our data, for example, in Fig. 5(b). Moreover, this type of asymmetry disappears for lower values of the critical field, where surface superconductivity has disappeared,[8] for example, in Fig. 5(c).

Flux-flow heating of the sample leads to a similar asymmetry between the ascending and descending field branches. On increasing fields, the negative ΔT is reduced, and on decreasing fields, the positive ΔT increased. An order of magnitude estimate of flux-flow heating can be obtained on the basis of the Bardeen-Stephen model.[19] For a cylindrical sample of radius R, length L, and for smooth field ramping at a rate dH/dt, one obtains $P_{ff} \approx 10^7 (dH/dt)^2 \pi R^4 L/(8\rho_{ff})$. This turns out to be negligible for the field ramp rates, approximately 1 Oe/s, used in our measurements. We show the effect of this mechanism, grossly exaggerated, in Fig. 9(b). Between the above two sources of irreversible heating, it is clear that low field ramp rates will render the latter $[\propto (dH/dt)^2]$ negligible, but will not reduce the effect of the former which scales as dH/dt, as does the magnetocaloric ΔT.

Next, we examine the case of a nonequilibrium critical state profile outside the peak-effect region. A critical current that monotonically decreases with field, i.e., away from the peak-effect region, will result in the opposite asymmetry than the one just mentioned. This is so because on increasing fields, the critical state profile becomes less steep, resulting in faster loss of flux than the field ramp rate and thus increased ΔT. The opposite occurs on decreasing fields, resulting in a lower ΔT than indicated by the equilibrium $T_s(\partial s/\partial H)_T$. This mechanism is shown schematically in Fig. 9(d). A simplified calculation for cylindrical sample geometry, such as the ones found in the literature,[20,37] yields an asymmetry factor in ΔT equal to (cgs units)

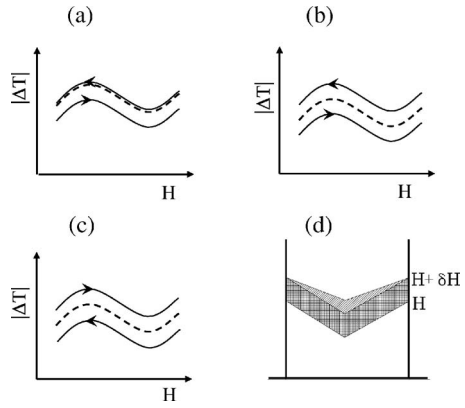

FIG. 9. [(a)–(c)] Schematic representations of the asymmetries induced by irreversible and nonequilibrium effects on the magnetocaloric measurement, $|\Delta T|$. The field-ramp directions are indicated by arrows, and the equilibrium $(\partial s/\partial H)_T$ curve corresponds to the dashed line. (a) Surface barrier heating. (b) Flux-flow heating. (c) Critical state screening. (d) Qualitative schematic of the evolution of the critical state field profile for increasing field and $\partial j_c/\partial H < 0$. When the applied field increases from H to $H+\delta H$, the flux increase corresponds to the total shaded area, and not just the lower shaded part. This results in increased magnetocaloric signal, as shown in (c) and discussed in the text.

$$1 \pm (4\pi R/3c)(\partial J_c/\partial H)_T \tag{A1}$$

for increasing $(-)$ and decreasing $(+)$ fields. Here, R is the sample radius and $J_c(H)$ the H dependent critical current.

To see how this factor arises, consider a cylindrical sample geometry, with the field applied along the cylindrical axis. The critical current is taken to depend on B, or equivalently on H. We focus on the region close to H_{c2}, where these are linearly related by $B=(1+1/\zeta)H-H_{c2}/\zeta$, with $\zeta=\beta_A(2\kappa^2-1)$.[22] Due to critical current screening, the local induction (or field) inside the sample is modified with respect to the applied field and depends on radial distance from the axis (r) of the sample: $H=H(r)$. From the Ampère law, the field variation resulting from the critical current is

$$\frac{dH}{dr} = \pm \frac{4\pi}{c} J_c(H(r)),$$

for increasing $(+)$ and decreasing $(-)$ fields. The critical current depends on B, but we make the simplifying assumption that for a given value of applied field H_a, the local induction inside the sample leads to a negligible critical current variation: $J_c(r)=J_c=$const. In addition, we neglect demagnetizing effects. We then obtain

$$H(r) = H_a \pm (4\pi/c) J_c (r-R),$$

where R is the sample radius and again the solutions correspond to increasing $(+)$ and decreasing $(-)$ fields. The corresponding magnetic induction is simply

$$B(r) = \left\{ H_a \pm \frac{4\pi}{c} J_c (r - R) \right\} \left(1 + \frac{1}{\zeta} \right) - \frac{H_{c2}}{\zeta}.$$

This is easily integrated over the cross-sectional area of the sample in order to obtain the following magnetic flux through the sample:

$$\Phi = \left\{ H_a \left(1 + \frac{1}{\zeta} \right) - \frac{H_{c2}}{\zeta} \mp \left(1 + \frac{1}{\zeta} \right) \frac{4\pi R J_c}{3c} \right\} \pi R^2. \quad \text{(A2)}$$

Note that here the significance of the signs is reversed for increasing (−) and decreasing (+) fields. The rate of change in magnetic flux through the sample for changes in applied field is

$$\frac{d\Phi}{dH_a} = \left\{ 1 \mp \frac{4\pi R}{3c} \left(\frac{\partial J_c}{\partial H} \right)_T \right\} \left(1 + \frac{1}{\zeta} \right) \pi R^2.$$

This is proportional to the magnetocaloric signal and includes the asymmetry factor given in Eq. (A1), with negative (−) sign for increasing field and positive (+) for decreasing field.

*Corresponding author. Electronic address: nikos@brown.edu
†Corresponding author. Electronic address: xsling@brown.edu

[1] A. I. Larkin, Sov. Phys. JETP **31**, 784 (1970); Y. Imry and S. Ma, Phys. Rev. Lett. **35**, 1399 (1975).
[2] T. Nattermann, Phys. Rev. Lett. **64**, 2454 (1990).
[3] T. Giamarchi and P. Le Doussal, Phys. Rev. Lett. **72**, 1530 (1994).
[4] D. K. Christen, F. Tasset, S. Spooner, and H. A. Mook, Phys. Rev. B **15**, 4506 (1977).
[5] X. S. Ling, S. R. Park, B. A. McClain, S. M. Choi, D. C. Dender, and J. W. Lynn, Phys. Rev. Lett. **86**, 712 (2001).
[6] A. M. Troyanovski, M. van Hecke, N. Saha, J. Aarts, and P. H. Kes, Phys. Rev. Lett. **89**, 147006 (2002).
[7] W. DeSorbo, Rev. Mod. Phys. **36**, 90 (1964).
[8] S. R. Park, S. M. Choi, D. C. Dender, J. W. Lynn, and X. S. Ling, Phys. Rev. Lett. **91**, 167003 (2003).
[9] M. G. Adesso, D. Uglietti, R. Flukiger, M. Polichetti, and S. Pace, Phys. Rev. B **73**, 092513 (2006).
[10] D. Jaiswal-Nagar, D. Pal, M. R. Eskildsen, P. C. Canfield, H. Takeya, S. Ramakrishnan, and A. K. Grover, Pramana, J. Phys. **66**, 113 (2006).
[11] R. L. Cormia, J. D. Mackenzie, and J. D. Turnbull, J. Phys. Chem. **65**, 2239 (1963); R. W. Cahn, Nature (London) **323**, 667 (1986).
[12] R. Lortz, F. Lin, N. Musolino, Y. Wang, A. Junod, B. Rosenstein, and N. Toyota, Phys. Rev. B **74**, 104502 (2006).
[13] N. Daniilidis (unpublished).
[14] Y. Shapira and L. J. Neuringer, Phys. Rev. **154**, 375 (1967).
[15] I. K. Dimitrov, Ph.D. thesis, Brown University, 2007.
[16] A. T. Fiory and B. Serin, Phys. Rev. Lett. **16**, 308 (1966); F. A. Otter, Jr. and P. R. Solomon, *ibid.* **16**, 681 (1966).
[17] Note that Eq. (1) can be simplified to the form $\Delta T = A\dot{H} + B\Delta T$. The harmonic response to $H = H_0 e^{i\omega t}$ is determined by the magnetocaloric term $\Delta T \approx i\omega A H_0 e^{i\omega t}$ at low frequencies, $\omega B \ll 1$.
[18] C. P. Bean and J. D. Livingston, Phys. Rev. Lett. **12**, 14 (1964).
[19] J. Bardeen and M. J. Stephen, Phys. Rev. **140**, A1197 (1965).
[20] C. P. Bean, Phys. Rev. Lett. **8**, 250 (1962).
[21] P. G. deGennes, Solid State Commun. **3**, 127 (1965).
[22] P. G. deGennes, *Superconductivity of Metals and Alloys* (Benjamin, New York, 1966).
[23] S. P. Farrant and C. E. Gough, Phys. Rev. Lett. **34**, 943 (1975).
[24] D. J. Thouless, Phys. Rev. Lett. **34**, 946 (1975).
[25] R. Lortz, N. Musolino, Y. Wang, A. Junod, and N. Toyota, Phys. Rev. B **75**, 094503 (2007).
[26] J. C. Wheeler, Phys. Rev. A **12**, 267 (1975).
[27] D. S. Fisher, M. P. A. Fisher, and D. A. Huse, Phys. Rev. B **43**, 130 (1991).
[28] A possible change of vortex entropy at the peak effect is expected to be very small, if present, and is certainly not detectable with our technique.
[29] R. B. Griffiths, Phys. Rev. Lett. **23**, 17 (1969).
[30] T. Vojta, J. Phys. A **39**, R143 (2006).
[31] D. Li and B. Rosenstein, Phys. Rev. B **70**, 144521 (2004).
[32] T. Nattermann and S. Scheidl, Adv. Phys. **49**, 607 (2000).
[33] S. Mohan, J. Sinha, S. S. Banerjee, and Y. Myasoedov, Phys. Rev. Lett. **98**, 027003 (2007).
[34] N. Q. Lam, P. R. Okamoto, and M. Li, J. Nucl. Mater. **251**, 89 (1997).
[35] J. R. Clem, *Low Temperature Physics-LT13*, edited by K. D. Timmerhaus, W. J. O'Sullivan, and E. F. Hammel (Plenum, New York, 1974), Vol. 3, p. 102.
[36] L. Burlachkov, Phys. Rev. B **47**, 8056 (1993).
[37] Ming Xu, Phys. Rev. B **44**, 2713 (1991).